Supporting Information

Generation of Antibubbles from Core–Shell Double Emulsion Templates Produced by Microfluidics

*Justin E. Silpe,[†,‡] Janine K. Nunes,[‡] Albert T. Poortinga,[§] and Howard A. Stone[‡],**

[†]Department of Macromolecular Science and Engineering, University of Michigan, Ann Arbor, Michigan 48109, United States

[‡]Department of Mechanical and Aerospace Engineering, Princeton University, Princeton, New Jersey, 08544, United States

[§]FrieslandCampina Research, Harderwijkerstraat 6, 7418 BA Deventer, The Netherlands

Movie S1: Continuous production of W/O/W emulsions with relatively high oil volume fractions. Devices were secured on to the stage of an inverted microscope (Leica DMI4000B), and the process was viewed in real time. The stage is moved (screen left to right) in order to capture the entire production starting at the first junction and ending downstream (screen right) from the second junction.

Movie S2: Extended media used for Figure 5. CLSM video of antibubble collapse in the presence of 0.5 wt% Tween 80. Bright-field and fluorescence footage was recorded concurrently using CLSM and are presented side by side in the current clip (left and right respectively).

Movie S3: Production of thin-shelled W/O/W emulsions using the same (CFF) microfluidic device geometries. Shell thickness was controlled by adjusting flow rates of the outer and middle fluids relative to the inner phase. A typical flow rate for thin-shelled W/O/W emulsions was 1.5 μL/min, 4 μL/min, and 40 μL/min respectively. Due to the significantly greater rates of production, footage was captured at 1100 fps using a high-speed video camera (Phantom V7.3, Vision Research) mounted to the inverted microscope at the of production. The stage was held stationary at the second flow-focusing junction to confirm the formation of thin-shelled W/O/W structures. Playback speed was increased 250% prior to encoding at 10 fps.

Movie S4: High-speed, fluorescence video of thin-shelled W/O/W emulsions produced at the second flow focusing junction. The fluorescence channel allows for the positive identification of Nile Red in the middle phase as a thin oil shell. Video was recorded at the same position on the microfluidic device in Movie S3 (bright-field) as Movie S4 (fluorescence), however under the reduced frame rate of 300 fps (in order to increase gain/resolution of fluorescence, Movie S4). Video was encoded at 10 fps.

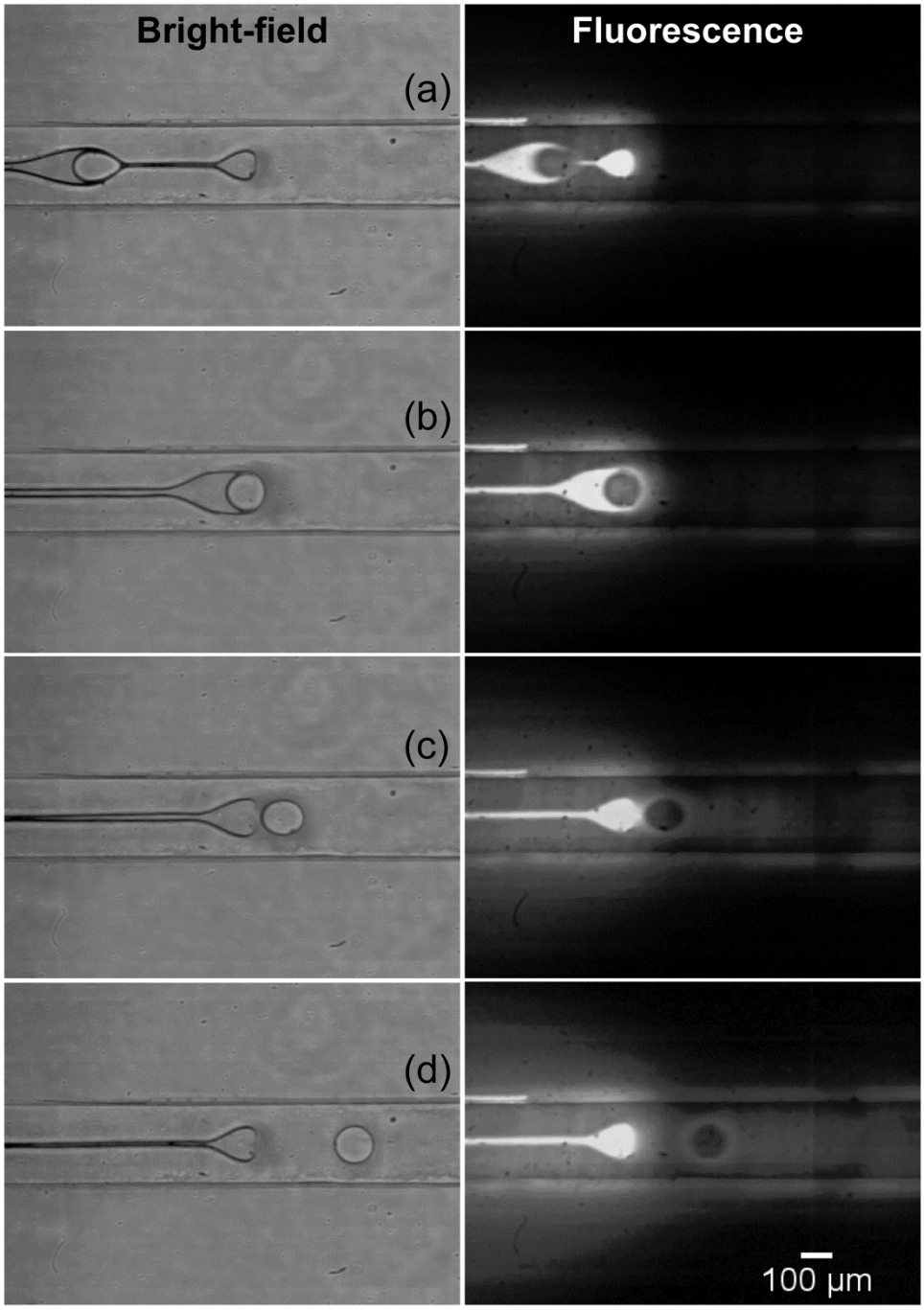

Figure S5: Formation of thin-shelled W/O/W emulsions at the second flow-focusing junction. (Left) Bright-field and (right) fluorescence images, rendered from high-speed camera footage of S3 and S4 respectively, and arranged vertically **(a-d)**, depicting the breakup of W/O to W/O/W with thin oil shells. Because bright-field and fluorescence images were taken independently and at different frame rates, (left) and (right) do not correspond to identical time points or droplets.

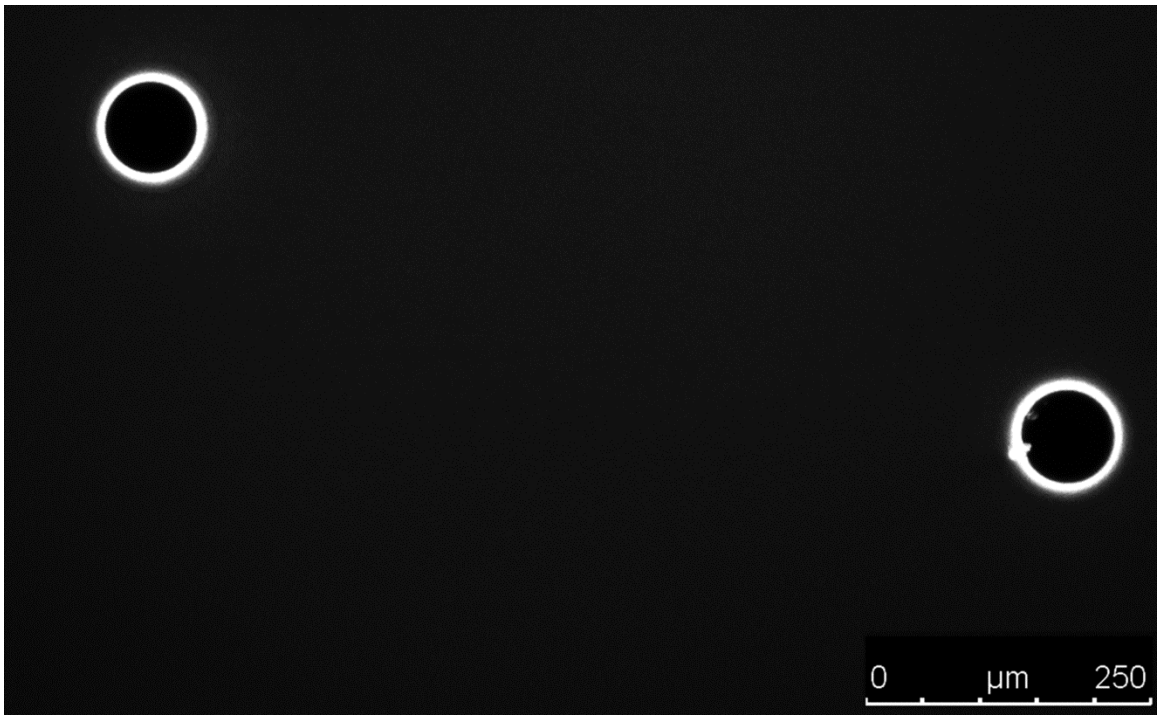

Figure S6: Fluorescence micrograph of thin-shelled W/O/W emulsions after freeze-drying and redispersing in DI water. Despite the significant change in relative volume fractions between thin and thick shells (see Figure 4 for example), absolute dimensions for the combined core-shell structures are comparable.

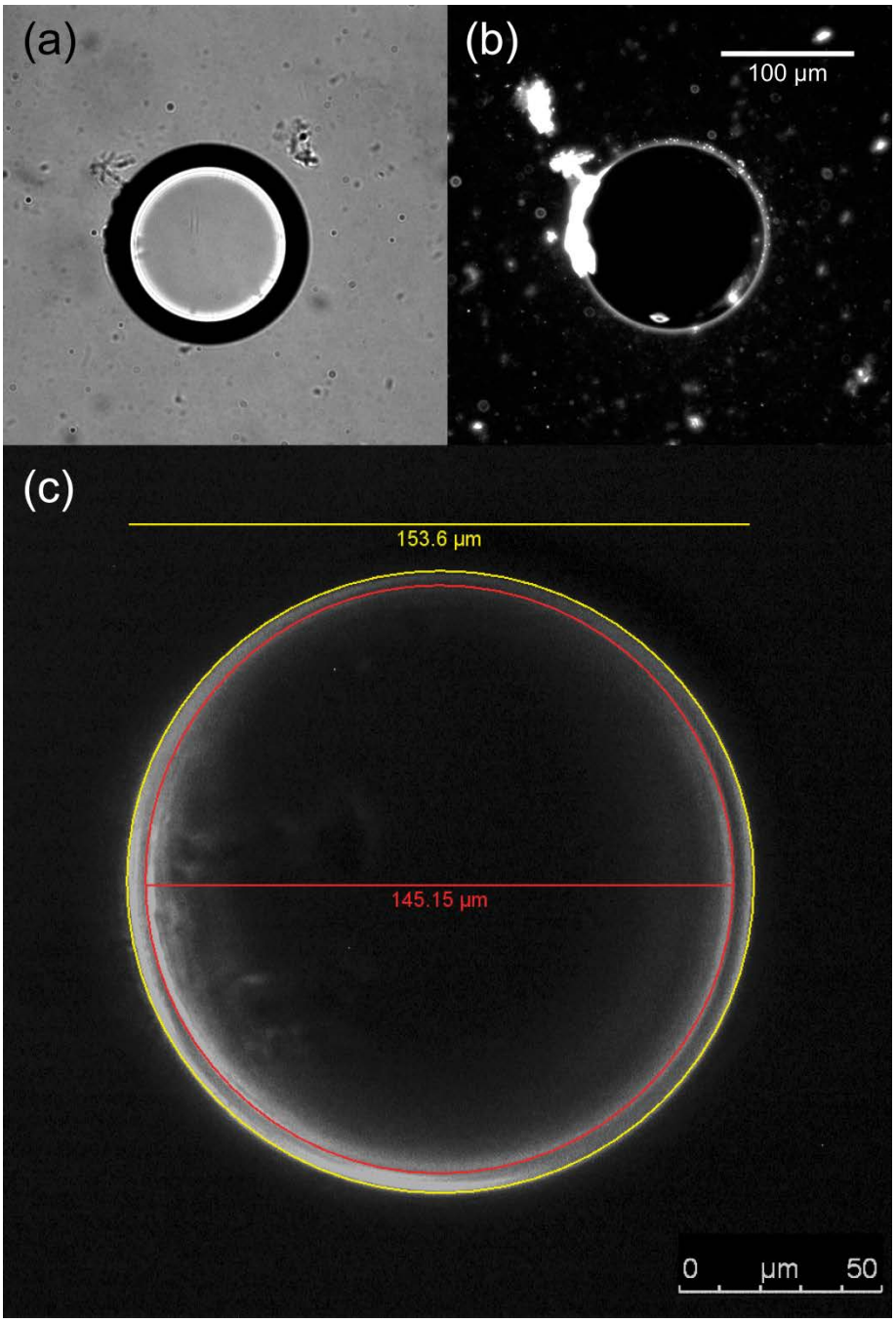

Figure S7: Higher objective **(a)** bright-field, **(b)** fluorescence, and **(c)** phase-contrast micrographs of a thin-shelled W/O/W emulsion after freeze-drying and redispersing in DI water. In contrast to antibubbles stemming from W/O/W templates of relatively high oil fractions, thin-shelled oil layers appear to result in only a single layer between the core and continuous phase, as evidenced by the illuminated ring of Nile Red in the (b) fluorescence micrograph. The phase contrast micrograph (c) was used to estimate the inner and outer core-shell volume. The shell volume fraction of thin-shelled freeze-dried and reconstituted material was less about 0.15. In this way, shell volume fraction was varied over a 5-fold range, from 0.15 for the thin-shelled

material to 0.79 for that of the higher volume antibubbles. Though mentioned in the main text, the individual phase compositions of the thin-shelled material could not be discerned on the basis of microscopy. Given the apparent core-shell structure, possible constructions would include aqueous-air (i.e. antibubbles), solid-solid, aqueous-solid, and air-solid (i.e. solid stabilized bubbles) with particular resemblance to those of Dickinson et al.[1]

Determination of emulsion and antibubble diameters

As noted in the main text, diameters were measured using image analysis software (ImageJ, National Institutes of Health, Bethesda, MD). In the case of non-spherical structures, which were occasionally found for reconstituted antibubbles, diameters were calculated by dividing the perimeter (regardless of geometry) by π.

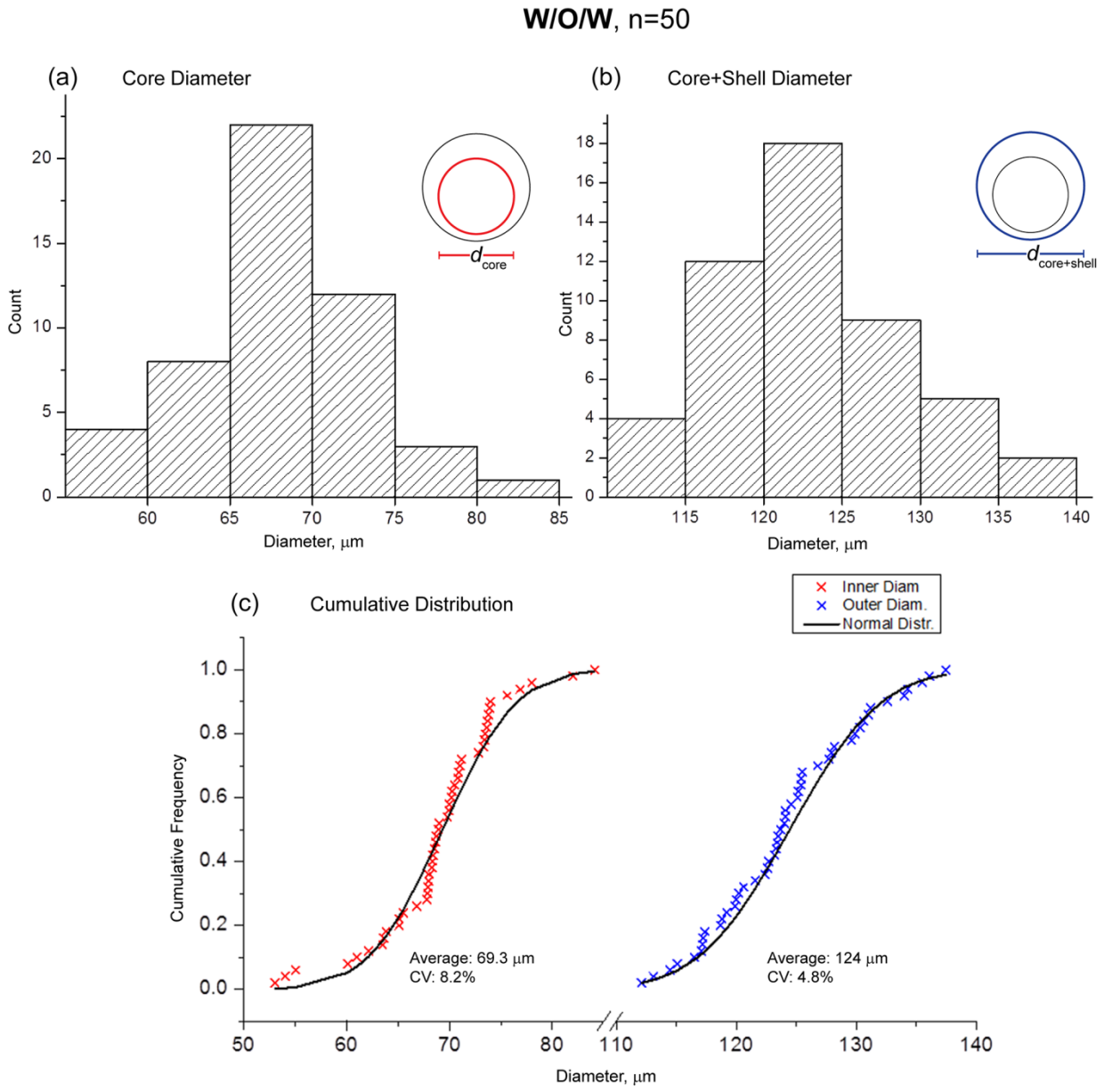

Figure S8: Histogram of W/O/W **(a)** core and **(b)** core+shell diameter distributions. **(c)** Cumulative distribution functions of core (left, red) and core+shell (right, blue) dimensions, each against a normal distribution (black).

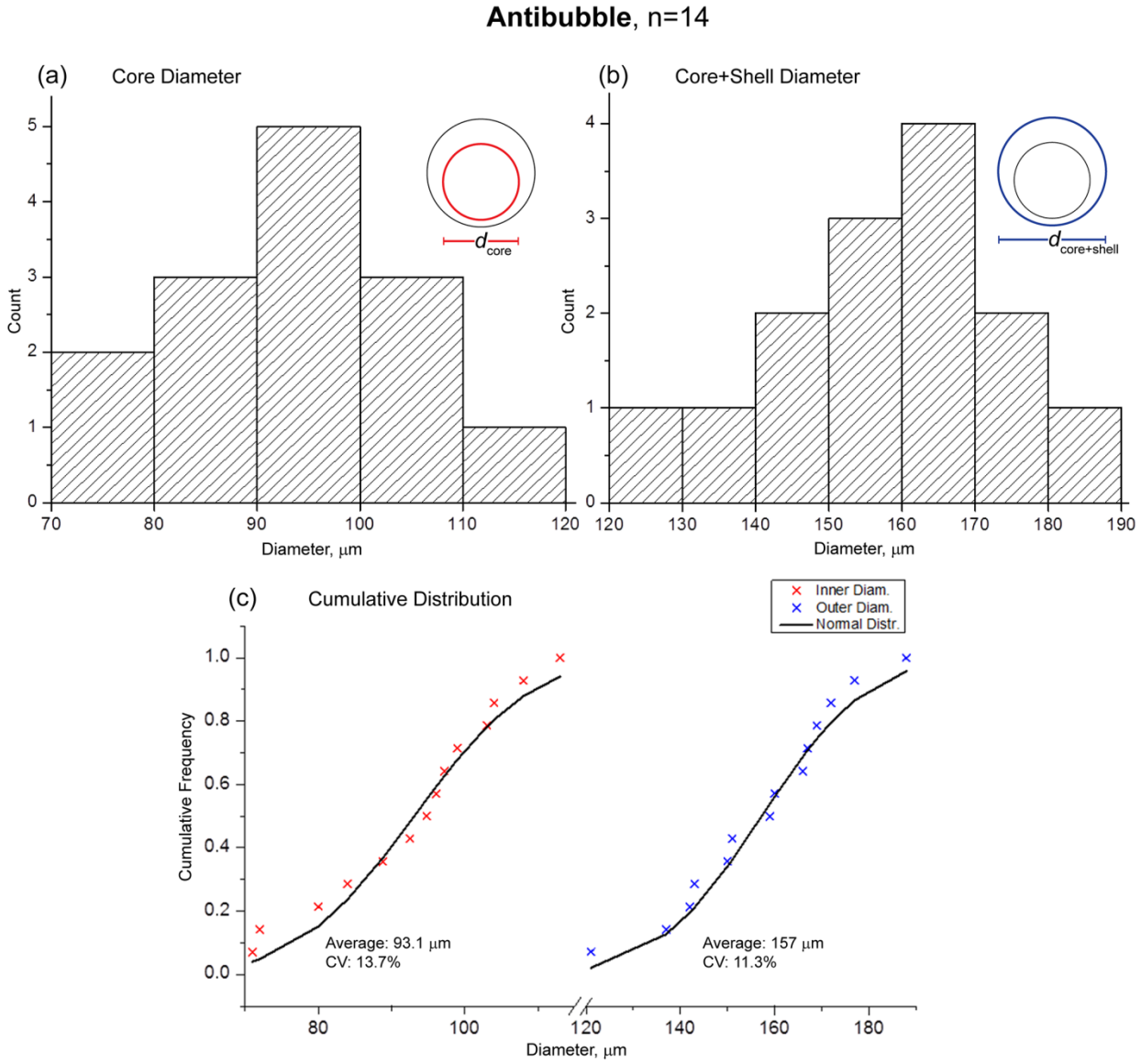

Figure S9: Histogram of antibubble **(a)** core and **(b)** core+shell diameter distributions. **(c)** Cumulative distribution functions of core (left, red) and core+shell (right, blue) dimensions, each against a normal distribution (black). To limit batch-to-batch variability, all antibubble dimensions were calculated from the same initial batch of W/O/W sample shown in Figure S8 in a single reconstitution. Sample size is necessarily reduced from Figure S8 to S9 as a result of reconstituting only a fraction of the freeze-dried product onto a single glass slide at a time. In addition, antibubbles do not frequently pack as efficiently as the initial W/O/W emulsion which further limited the number of antibubbles imaged.

REFERENCES

(1) Dickinson, E.; Ettelaie, R.; Kostakis, T.; Murray, B. S. Factors controlling the formation and stability of air bubbles stabilized by partially hydrophobic silica nanoparticles. *Langmuir* **2004**, *20*, 8517–8525.